PAPER

Check for updates

Exciton annihilation and diffusion length in disordered multichromophoric nanoparticles†

Amira Mounya Gharbi, [ID] [a] Deep Sekhar Biswas, [b] Olivier Crégut, [a] Pavel Malý, [ID] [c] Pascal Didier, [ID] [b] Andrey Klymchenko [ID] [b] and Jérémie Léonard [ID] *[a]

Efficient exciton transport is the essential property of natural and synthetic light-harvesting (LH) devices. Here we investigate exciton transport properties in LH organic polymer nanoparticles (ONPs) of 40 nm diameter. The ONPs are loaded with a rhodamine B dye derivative and bulky counterion, enabling dye loadings as high as 0.3 M, while preserving fluorescence quantum yields larger than 30%. We use time-resolved fluorescence spectroscopy to monitor exciton–exciton annihilation (EEA) kinetics within the ONPs dispersed in water. We demonstrate that unlike the common practice for photoluminescence investigations of EEA, the non-uniform intensity profile of the excitation light pulse must be taken into account to analyse reliably intensity-dependent population dynamics. Alternatively, a simple confocal detection scheme is demonstrated, which enables (i) retrieving the correct value for the bimolecular EEA rate which would otherwise be underestimated by a typical factor of three, and (ii) revealing minor EEA by-products otherwise unnoticed. Considering the ONPs as homogeneous rigid solutions of weakly interacting dyes, we postulate an incoherent exciton hoping mechanism to infer a diffusion constant exceeding 0.003 cm² s⁻¹ and a diffusion length as large as 70 nm. This work demonstrates the success of the present ONP design strategy at engineering efficient exciton transport in disordered multichromophoric systems.

Introduction

The transport of electronic excitation energy – excitons – is the function of so-called Light-Harvesting (LH) organic materials. In natural LH pigment-protein complexes, a subtle balance between structural organisation and disorder results in a partial delocalisation of electronic excitation over a few nearby pigments and a remarkably efficient exciton transport directed towards the photosynthetic reaction center.[1–5] In synthetic organic materials, the efficiency of light energy conversion remains limited by exciton transport to a donor–acceptor interface, where electron–hole charge separation may occur.[6–8] The recent use of non-fullerene acceptors enabling a larger exciton diffusion length – *i.e.* beyond the typical 5 to 10 nm range – was essential to improve significantly the efficiency of organic photovoltaic energy conversion[9–12] or photocatalysis.[13,14]

Much larger singlet exciton diffusion lengths – with diffusion constants approaching or exceeding 1 cm² s⁻¹ – have

been reported in structurally well organized, molecular aggregates or crystals,[15–19] possibly also enabling directed transport.[20,21] In such systems, tight molecular packing and large dye interactions favor the quantum delocalisation of electronic excitation over multiple sites.[22–24] As a limiting case of such a behavior, macroscopic exciton coherence, *i.e.* quantum delocalisation over the entire length (≃10 μm) of a highly-ordered single polymer chain was demonstrated at 10 K.[25] Conversely, static or dynamic disorder promotes excitation energy localisation on individual sites. In the corresponding limiting case (*e.g.* weakly interacting dyes in solution), exciton transport results from the incoherent hopping of electronic excitation,[26] where individual hopping events are described by the Förster model for Resonant Energy Transfer (FRET) from a dye in its first excited singlet (S_1) state to a nearby dye in its ground (S_0) state. Remarkable exciton transport properties have been reported at room temperature, *e.g.* along 1D supra-molecular aggregates, and proposed to result from a "combined coherent–incoherent motion",[16] such as an incoherent hoping of excitons delocalised over few units,[18,27] in line with the exciton transport mechanism described in natural LH complexes.[28] In less ordered systems, transient exciton delocalisation is introduced as a mechanism to explain exciton transport outperforming the prediction of the incoherent hopping model.[19,29,30]

[a] IPCMS, Université de Strasbourg – CNRS, Strasbourg, France.
E-mail: jeremie.leonard@ipcms.unistra.fr
[b] LBP, Université de Strasbourg, Illkirch, France
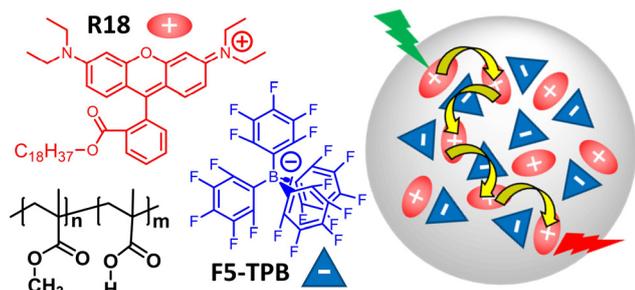*[c] Charles University, Prague, Czech Republic*

Fig. 1 Chemical structures of dye (R18) with its bulky counter ion (F5-TPB) and polymer (PMMA–MA) constituting dye-loaded polymeric, light-harvesting nanoparticles sketched on the right-hand side.

In this paper, we investigate fluorescent, dye-loaded polymer organic nanoparticles (ONPs), as a model for a disordered, weakly interacting multi-chromophoric system exhibiting remarkable exciton transport properties. Originally designed to produce high-brightness nanoprobes for bioimaging and biosensing applications,[31,32] the polymer ONPs encapsulate cationic rhodamine B dye derivatives – see Fig. 1 – together with bulky counterions used to prevent dye aggregation and mitigate aggregation-caused fluorescence quenching (also called "self-quenching").[33,34] Depending on the polymer used, the ONPs exhibit various photophysical properties indicative of very efficient exciton transport, such as a collective fluorescence on/off switching,[35] similar to that observed *e.g.* in molecular J-aggregates.[36] Here, we use poly(methyl methacrylate-*co*-methacrylic acid) (PMMA–MA) as the polymer and the dyes are argued to be distributed homogeneously inside the ONP,[37] like in a disordered, rigid solution. Still sub-ps electronic energy transfer between chromophores is observed, indicating a very efficient exciton transport held responsible for a "giant" antenna effect,[38] with promising application to single (bio)molecule detection.[39]

Among various methods to characterise exciton transport in organic materials,[40,41] exciton–exciton annihilation (EEA) is a process controlled by exciton transport and exciton–exciton interactions, which results in an acceleration of the exciton population decay kinetics with increasing light excitation power. EEA has been investigated with a variety of experimental techniques including steady-state or time-resolved photoluminescence spectroscopy,[40,42–46] photon antibunching,[47–50] transient absorption spectroscopy,[9,10,18,51–57] time-resolved fluorescence up-conversion,[58,59] coherent multi-dimensional electronic spectroscopy[60,61] and related "intensity cycling" transient absorption spectroscopy.[62] Here we propose to investigate the exciton diffusion properties in these dye-loaded ONPs by monitoring EEA *via* time-resolved photoluminescence detection, as a function of excitation power.

The mechanism commonly described for EEA in organic materials is an energy transfer[47–49] between two "colliding" excitons, producing one electronic ground state S_0, and one higher-lying electronic state S_p, with $p > 1$. In general, S_p is very short-lived and decays back to S_1 *via* internal conversion (IC)

on the sub-100 fs time scale. Therefore, the exciton population $n(t)$ is modelled according to the following rate equation:[40,42,54,57,63,64]

$$\frac{dn(t)}{dt} = -kn(t) - \frac{\gamma(t)}{2}n^2(t), \tag{1}$$

where k is the excited state (S_1) decay rate of isolated excitons, γ is the EEA rate associated to bimolecular exciton interactions, and the factor $1/2$ in the last term accounts for the fact that only one out of two interacting excitons is lost, assuming quantitative IC from S_p to S_1.[42,57] The general solution of eqn (1) is:

$$n(t) = \frac{n_0 \exp(-kt)}{1 + n_0 h(t)},$$
$$\text{with} \quad h(t) = \int_0^t \frac{\gamma(t')}{2}\exp(-kt')dt'. \tag{2}$$

Because of the bimolecular term $\propto n^2(t)$ in eqn (1), the exciton population decay kinetics depends non-linearly on the initial exciton density n_0, hence on the intensity of the excitation light pulse. Since the detected signal is integrated over the detection volume, the non-uniform transverse intensity profile of the excitation light pulse must be taken into account to enable a quantitative analysis of the observed population decay kinetics.[64] In other words – and in contrast to the vast majority of the photoluminescence investigations of EEA reported in the literature – one may in general not expect eqn (2) to reproduce the observed decay kinetics unless special excitation (*e.g.* flat excitation profile) or detection schemes are implemented.

Here, after deriving the analytical expression for the fluorescence decay kinetics actually expected for an ensemble of ONPs in solution with a Gaussian excitation profile, we propose a simple confocal detection scheme in order to restrict the actual detection volume to the central part of the excitation volume where the initial exciton density is nearly uniform. Only then can we fit the data with eqn (2).[65] We demonstrate that the decay kinetics recorded with and without the confocal detection scheme are indeed qualitatively different, while fits of either dataset with the appropriate function give the same result for the EEA rate, within experimental reproducibility. We also show that overlooking this experimental issue leads to a systematic underestimate of γ, by a factor of two to three typically, and possibly more depending on the excitation beam intensity profile.

In addition, in the ONPs loaded with the largest dye concentration, we observe a shortening of the exciton lifetime upon increasing the excitation power, with a threshold effect indicating a very non-linear power dependence. Importantly, this phenomenon remains unnoticed without the confocal detection scheme. The observed decay kinetics are nicely reproduced with a modified model where quenchers Q are formed with low yield as by-products of EEA, *via* a minor S_p decay channel competing with IC. The exciton decay rate k then increases with the quencher density due to $S_1 - Q$ colli-

sional quenching, in perfect analogy with previous observations of exciton lifetime shortening due to singlet–triplet exciton annihilation in conjugated polymers.[66]

Eventually, all our data are nicely fitted with a time-independent γ coefficient, in line with the efficient exciton diffusion expected in these ONPs.[38] In fact, we observe that excitation probabilities as low as 0.1% – meaning no more than few excitons on average per nanoparticle – are enough to observe the signature of EEA, demonstrating the effective diffusion of excitons within the entire nanoparticle on a time scale shorter than their natural lifetime.

Dimensional analysis reveals that γ is proportional to the product DR_e of the exciton diffusion coefficient D and an effective distance R_e, interpreted as the distance at which excitons should approach to annihilate.[40,67] Measuring γ is therefore not enough to infer D: "additional information is required to separate motional (D) and interaction (R_e) effects".[40] Recently, the independent measurements of D and γ revealed the coherent suppression of exciton–exciton interaction at low temperature in highly ordered molecular crystals.[46,68] However, when knowing only γ, a model to describe EEA must be postulated in order to evaluate D. Here, we assume the validity of the FRET, and evaluate R_e as a function of the Förster radius R_{EEA} associated with electronic excitation energy transfer between two excitons.[69–71] We perform complementary transient absorption spectroscopy (TAS) to determine R_{EEA} from the overlap between the excitons (S_1) absorption and emission spectra. Eventually we evaluate $D = 300$ nm^2 ns^{-1} = 0.003 cm^2 s^{-1}, a value more than one order of magnitude larger than in previously reported dye-loaded PMMA films,[57,72] thus validating the success of the present ONP design strategy

to synthesize disordered multi-chromophoric systems acting as efficient LH materials.

Materials and methods

Nanoprecipitation is used to encapsulate rhodamine B octadecyl ester (R18) and its counterion tetrakis(pentafluorophenyl) borate (F5-TPB) in nanoparticles of poly(methyl methacrylate-*co*-methacrylic acid) (PMMA–MA) polymer, as described elsewhere.[38] The average diameter of the organic nanoparticles (ONPs) is measured by transmission electron microscopy to be $\simeq 40$ nm, with a dispersion of $\pm 20\%$. Nanoparticles labelled ONP30 and ONP100 are produced with dye concentrations of, respectively, 30 wt% and 100 wt%, expressed as the mass of dye and counterion (R18/F5-TPB) relative to the mass of the polymer. This corresponds to R18 dye molar concentrations of 0.17 M and 0.36 M, respectively. Two distinct batches A and B of each type of nanoparticle have been synthesized and investigated in distinct measurement campaigns, to demonstrate the reproducibility of the results below.

Fig. 2 illustrates the experimental scheme for time-resolved fluorescence (TRF) spectroscopy. In short (see the details in the ESI†), a 300 fs laser pulse centered at 515 nm is used to excite the fluorescence of ONP30 and ONP100 dispersed in water to a typical absorption coefficient of 0.5 mm^{-1} or less at 515 nm. The laser system (Tangerine, by Amplitude) enables tuning the repetition rate from 100 kHz to 100 Hz when changing the excitation pulse energy from low to high, respectively. The solutions are circulated in a flow cell of thickness $l = 0.2$ or 0.5 mm. A streak camera is used to monitor the fluo-
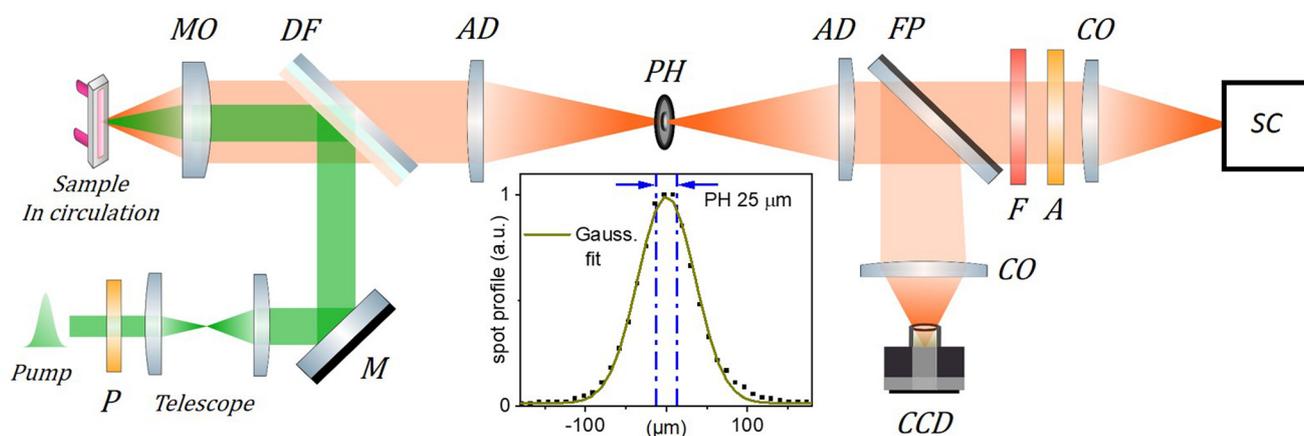

Fig. 2 Scheme of the TRF setup. The 515 nm, 300 fs excitation (pump) beam is collimated and its diameter adjusted to 1.3 mm FWHM using a telescope. It is then reflected by a dichroic filter (DF) and focused by a microscope objective (MO, Mitutoyo Plan Apo 10X, f = 20 mm, NA = 0.28, pupil diameter = 11.2 mm) in the circulated sample solution. The emitted fluorescence is collected by the same MO and transmitted through the DF to the "confocal setup" composed of two achromatic doublets (AD, f = 100 mm) and a 25 μm pinhole (PH) used to spatially filter the fluorescence signal. A streak camera (SC, Hamamatsu Streakscope C10627) working in single photon counting mode is used for detection under magic angle configuration (P: polarizer, A: analyzer; F: long pass filter; CO: camera objectives). In addition, a flip mirror (FP) and a CCD camera are used to monitor the fluorescence spot intensity profile in the PH plane as shown in the inset (dots; PH removed) together with its Gaussian fit (green curve), and the 25 μm central region over which the fluorescence signal is detected when the PH is in place (blue dash-dotted lines). The actual excitation spot size in the sample plane is 5 times smaller than in the PH plane and must be carefully calibrated (see details in the ESI†) to evaluate accurately the initial exciton density n_0.

rescence decay kinetics with 10 ps time resolution (see Fig. S8 (B)†). The transverse profile of the laser pulse is nearly Gaussian and carefully measured by imaging the fluorescence spot with a conventional CCD camera, under very low excitation power to avoid EEA and saturation of the fluorescence intensity. At higher excitation power where EEA takes place, more EEA and faster decay kinetics will occur for ONPs located in the center of the excitation volume – where the pulse intensity and excitation probability are higher – than in the periphery. The decay kinetics actually monitored results from the average over the entire excitation volume. Alternatively, we may collect the fluorescence emission using a confocal detection scheme which allows us to overlap a pinhole with an intermediate real optical image of the excitation volume in order to detect only the fluorescence emitted from the central part of the excitation volume.

For a quantitative analysis of the observed decay kinetics, we define the excitation pulse energy profile as: $\varepsilon(x,y,z) = \frac{\varepsilon_0}{S} e^{-az} f(x,y)$, where ε_0 is the energy per pulse, $f(x,y)$ the transverse energy profile with $f(x = y = 0) = 1$ and $S = \int f(x,y) dx dy$ the pulse transverse section. The e^{-az} factor accounts for the pulse absorption along its propagation direction z inside the sample, with a the absorption coefficient. The assumption that the transverse beam profile $f(x,y)$ does not depend on z remains valid at the beam focus, provided that the Rayleigh length L exceeds the sample thickness l or light penetration depth. We typically have $L > 0.6$ mm $> l$ (see ESI† for details). The fluorescence emission of an ONP located in $\vec{r} = (x,y,z)$ within the excitation volume is proportional to its exciton population $n(\vec{r},t)$, which decays according to eqn (2), with an initial exciton density $n(\vec{r};t=0) = n_0 f(x,y) e^{-az}$ directly proportional to the energy pulse profile (see ESI†). The measured fluorescence decay kinetics is thus proportional to the integral $F(t)$ of $n(\vec{r},t)$ over the entire detection volume V:

$$F(t) = \frac{1}{V} \int \frac{n_0 e^{-az} f(x,y) \exp(-kt)}{1 + n_0 e^{-az} f(x,y) h(t)} d\vec{r}. \quad (3)$$

In the confocal detection scheme, the pinhole is used to restrict the detection volume V to only the central part of the excitation volume, i.e. x, y small enough that $f(x,y) \simeq 1$ inside V. In this case, the detected signal is, for a weakly absorbing sample ($al < 1$):

$$F_{PH}(t) = \frac{\tilde{n}_0 \exp(-kt)}{1 + \tilde{n}_0 h(t)}. \quad (4)$$

This is nothing but eqn (2), where n_0 is replaced by $\tilde{n}_0 = n_0 \times \frac{1 - e^{-al}}{al}$, the peak exciton density averaged along z over the sample thickness l, see ESI† for details. Hence, only for a flat excitation profile – or in the presence of a small-enough pinhole in the confocal detection scheme – do we expect to observe decay kinetics obeying eqn (2).

When removing the pinhole, the integration volume V extends to the entire excitation volume. For a Gaussian pulse profile, the integration can be written analytically (see ESI† for

details), and for a weakly absorbing sample, the measured decay kinetics is expected to obey:

$$F_{noPH}(t) = \frac{\exp(-kt)}{h(t)} \ln(1 + \tilde{n}_0 h(t)). \quad (5)$$

The light power dependence of the fluorescence decay kinetics predicted by eqn (4) or (5) are qualitatively different, and neglecting the effect of an inhomogeneous beam energy profile results in significant errors on the γ value, as illustrated in Fig. S4 in the ESI.† In the following, we report a series of fluorescence decay kinetics recorded as a function of excitation power on several ONP solutions produced from different synthetic batches. We compare the results obtained with and without the pinhole and fit the data with the functional forms given by eqn (4) or (5), respectively. As will be seen below, the exciton decay kinetics is nicely reproduced in all cases when postulating a time-independent γ value, meaning that $h(t) = (1 - \exp(-kt))/n_A$, where we define $n_A = 2k/\gamma$ the critical exciton density above which the exciton decay is dominated by EEA rather than natural S_1 lifetime. The determination of reliable γ values requires accurate calibration of the initial exciton density n_0, deduced from the R18 dye extinction coefficient – calibrated to $\varepsilon_{max} = 125\,000$ M^{-1} cm^{-1},[73] at $\lambda_{max} = 560$ nm – and from the dye number density ρ in the ONPs (see ESI† for details).

Results

Fig. 3(A) shows the absorption and emission spectra of ONPs with 0.5, 30 and 100 wt% dye-loading. We observe a slight increase in the intensity of the vibrational shoulder at 525 nm, indicating a relatively weak interaction between dyes despite the large dye concentration. The weak red shift of the fluorescence emission (by no more than 120 cm^{-1}), may also be due to dye–dye interactions. However, since the single nanoparticle absorbance approaches 0.15 at λ_{max} for the largest dye concentration, also reabsorption likely contributes to the observed fluorescence red-shift.

With low-enough excitation power where no EEA occurs, the exciton decay kinetics do not depend on the excitation power. Fig. 3(B) compares the fluorescence decay kinetics monitored at such low excitation powers on different samples. The decay kinetics are clearly not monoexponential, but correctly fitted with a sum of 3 exponential decay components (k_i, $i = 1$ to 3) representative of a distribution of exciton decay rates, itself indicative of a distribution of exciton sub-populations possibly related to structural disorder among ONPs. The results of the fits are displayed in Table 1 and show that all decay kinetics exhibit a consistent 4.3 ns long-lived component with a significant relative weight. Noticeably, this lifetime is that of low-loading ONPs showing a 99% fluorescence quantum yield.[38] We conclude, that even at much higher loadings, a significant sub-population of dyes (of 34% and 19% for ONP30 and ONP100, respectively) still keep a non-quenched fluorescence lifetime.
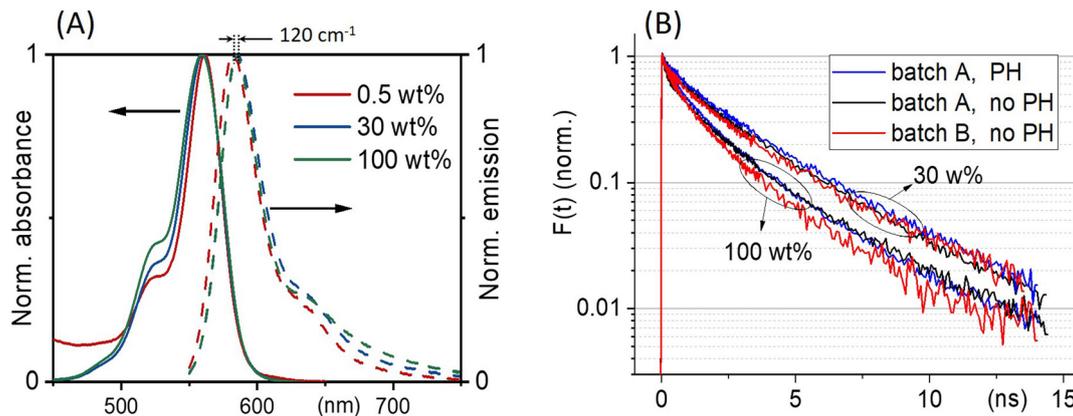
Fig. 3 (A) ONPs steady-state absorption and emission spectra as a function of R18/F5-TPB loading. (B) Comparison of the fluorescence decay kinetics recorded with (PH) or without (no PH) pinhole, at low excitation power where no EEA occurs, for two batches A and B of nanoparticles ONP30 and ONP100. The results of the tri-exponential fits of all these curves are disclosed in Table 1.

Table 1 Decay rates (k_i) and corresponding relative amplitudes (A_i) resulting from the triexponential fit of the fluorescence decay kinetics displayed in Fig. 3, together with the ensemble-averaged fluorescence lifetimes $\left(\langle\tau\rangle = \sum_i A_i/k_i\right)$ and quantum yields (QY), as a function of dye loading

	Triexp. fit amplitudes[a] (%)				
Loading (wt%)	$1/k_1$ (ns) 0.1 to 0.2	$1/k_2$ (ns) 1.35 ± 0.15	$1/k_3$ (ns) 4.3 ± 0.6	$\langle\tau\rangle$ (ns)	QY
0.5[b]	—	—	100	4.2	0.99
30	17 ± 2	49 ± 2	34 ± 2	2.35 ± 0.15	0.44 ± 0.02
100	22 ± 2	57 ± 2	19 ± 2	1.6 ± 0.2	0.32 ± 0.04

[a] All decay kinetics displayed in Fig. 3 are fitted independently and reveal similar decay rates within the specified error bars. [b] Values taken from ref. 38.

Fig. 4 compares the decay kinetics observed with ONP30A when increasing the excitation power, in two distinct experiments performed in the absence or presence of the pinhole in the confocal detection scheme. The excitation power dependence of the decay kinetics is qualitatively different in both experiments. The quantitative analysis is done as follows. In line with the above tree-component analysis of the low-power decay kinetics indicating a distribution of ONPs (or a distribution of domains within ONPs), we postulate a 3-component fitting function $K_{\text{PH/noPH}}(t)$, with three exciton decay rates (the k_i's evidenced above), but a common γ coefficient describing the exciton diffusion and interaction in all ONPs or domains:

$$K_{\text{PH/noPH}}(t) = \sum_{i=1}^{3} \alpha_i F_{\text{PH/noPH}}(k_i, \gamma, t),\qquad(6)$$

where $F_{\text{PH/noPH}}(k_i, \gamma, t)$ are defined by eqn (4) or (5) for data recorded in the presence or absence of the pinhole, respectively. In both fits (see ref. 65), the α_i and k_i values are very close and mostly determined by the low-energy data, while a unique γ parameter is enough to account for the faster decay at higher

energies. Importantly, neglecting the effect of averaging over the excitation volume and fitting the data recorded without pinhole with the function $K_{\text{PH}}(t)$ (see Fig. S10†) results in a γ value underestimated by a factor of 3. Including all results obtained with ONP30A (Fig. 4, panels A and B) and ONP30B (Fig. S10,† left panel), we conclude that for a dye loading of $\delta = 30\%$, we observe $\gamma = 5600 \pm 900$ nm^3 ns^{-1}.

With the 100 wt% dye-loaded ONPs, we observe a similar behavior up to intermediate excitation powers, but a shortening of the excitons lifetime for the highest excitation powers, as illustrated in Fig. 5. This observation is much more spectacular in the presence of the pinhole (compare Fig. 5A and C), as we collect the signal only from the center of the excitation volume, where the initial exciton density is the highest. To account for this observation, we need to modify the model proposed in eqn (1): we hypothesize the light-induced formation of long-lived quenchers Q at a density $n_Q(t)$ such that collisional quenching occurs with rate $\gamma_Q n_Q(t)$ and shortens the lifetime of the mobile excitons. Such a model is described by the following rate equations:

$$\begin{aligned}\frac{\mathrm{d}n(t)}{\mathrm{d}t} &= -(k + \gamma_Q n_Q(t))n(t) - (1+\beta)\frac{1}{2}\gamma n^2(t) + n_0 P(t)\\\frac{\mathrm{d}n_Q(t)}{\mathrm{d}t} &= \frac{\beta}{2}\gamma n^2(t)\end{aligned} \qquad(7)$$

where β is the fraction of doubly-excited dyes (S_p state, $p > 1$) formed via EEA, which would not undergo IC back to S_1 but a competing decay channel to Q. The term $n_0 P(t)$ accounts for laser-induced exciton formation kinetics, with $P(t)$ the instrument response function assumed to be Gaussian here.

The highly-excited singlet S_p state produced by EEA is very commonly assumed to decay quantitatively via IC to the S_1 state, justifying the factor 1/2 in the EEA-induced population decay term in eqn (1). However, in various conjugated polymers, other decay channels have been reported, which compete with IC: highly-excited singlet states produced either by sequential two photon absorption from sub-ps pulses or by
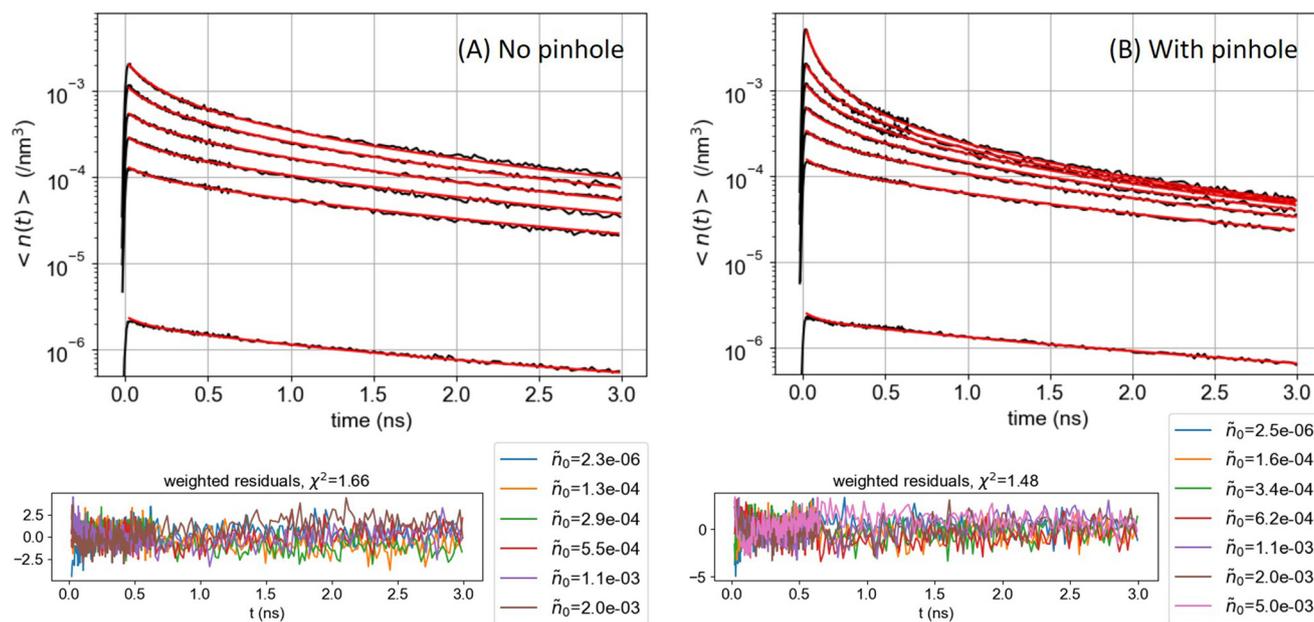
Fig. 4 ONP30, batch A: comparison of the exciton density (in nm^{-3}) decay kinetics averaged over the detection volume (A) without or (B) with the pinhole in the confocal detection scheme, for increasing excitation powers (see ESI† for the vertical axis calibration). The red lines are the result of the global fit of the decay kinetics with $K_{\text{noPH}}(t)$ for panel (A) and $K_{\text{PH}}(t)$ for panel (B), see eqn (6), yielding $\gamma = 6500$ and 4700 nm^3 ns^{-1}, respectively, with the residuals displayed in the lower panels.
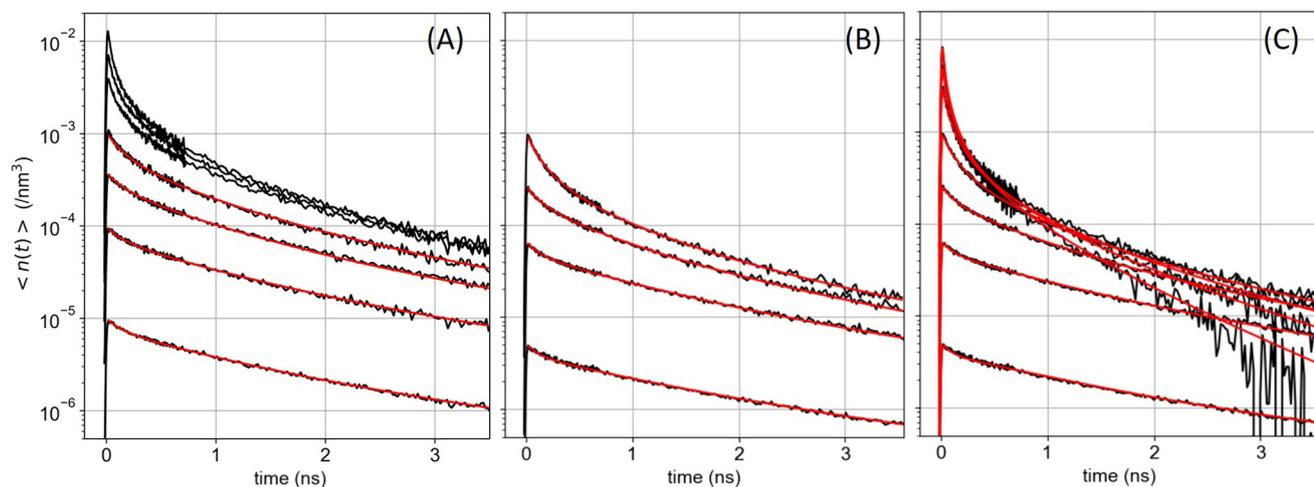

Fig. 5 ONP100, batch B: exciton density (in nm^{-3}) decay kinetics averaged over the detection volume (A) without or (B and C) with the pinhole in the confocal detection scheme, for increasing excitation powers. The red lines are the result of the global fit with three distinct models. In panel (A) the global fit is done with $K_{\text{noPH}}(t)$ while disregarding the decay traces recorded with the highest three excitation powers. In panel (B) the data are the same as in panel (C) but we disregard the highest three excitation powers and the global fit is performed with $K_{\text{PH}}(t)$. In panel (C) all decay traces are analyzed globally based on the model described by eqn (7), with $\beta = 0.024$ as a result of the fit (see text). The three analyses yield $\gamma = 7800$, 8300, 8030 nm^3 ns^{-1}, for panel A, B, and C, respectively.

EEA were observed to decay into charge-separated states[42,74–79] also referred to as molecular radical ions,[78] or into triplet states – *via* ultrafast singlet fission.[80,81] Single molecule spectroscopy of the rhodamine 6G fluorophore also evidenced photobleaching pathways from higher lying states (S$_{p>1}$),[82] as well as the photoproduction of both, long-lived triplet T$_1$ and reduced radical states.[83] For rhodamine B in ethanol, the T$_1$ and radical states happen to absorb at wavelengths $\lambda_{\text{max}} = 560$ nm and 550 nm, respectively – where the ground state S$_0$ also absorbs – with an extinction coefficient ε_{max} about 4 to 5 times weaker than that of the S$_0$ state.[84] The Förster radius R_Q for the exciton energy transfer to these species is thus close to $R_0/5^{1/6} \simeq 4$ nm, where R_0 is the Förster radius for homo-FRET evaluated from the spectral overlap of R18 emission and

absorption spectra (see ESI† for the evaluation of R_0). Hence, both the T_1 and radical states qualify as good exciton quenchers in the OPNs.

The exciton quenching (γ_Q) and annihilation (γ) rates in eqn (7) are related, since they describe diffusion-limited excitation energy transfer to a fixed quencher (with Förster radius R_Q) or to another diffusing exciton (with Förster radius R_{EEA}), respectively. Anticipating the Discussion section, we argue that $\gamma_Q = \gamma/2^{3/4} \times (R_Q/R_{EEA})^{3/2}$. If we assume $R_Q = 4$ nm and use the value derived below for R_{EEA}, we get $\gamma_Q \simeq \gamma/3$. Setting $\gamma_Q = \gamma/3$, and solving numerically the model described by eqn (7), yields fluorescence decay kinetics $F_Q(\beta,k,\gamma,t)$. In line with eqn (6) we again postulate a 3-component fitting function $K_Q(t) = \sum_i \alpha_i F_Q(\beta, k_i, \gamma, t)$ – with β and γ parameters common to all three sub-populations – to fit the data recorded in the presence of PH (where no additional averaging over the excitation volume is needed) as illustrated in Fig. 5C. The fitting procedure (see ref. 65) yields $\beta = 0.024$, and $\gamma = 8030$ nm^3 ns^{-1}.

An alternative model, where the quencher Q would be produced as a secondary decay channel directly from S_1 rather than from S_p does not reproduce the data so well (see ESI†). We conclude that a fraction of order 2% of the EEA events produce a byproduct Q, which is a good energy acceptor and reduces the exciton lifetime by collisional quenching. This result calls for scaling down by 2% the γ values obtained based on eqn (1) (where γ should be replaced by $(1 + \beta)\gamma$, even if no signature of Q is detectable). In the present case, this correction is anyway negligible compared to the experimental reproducibility. When performing the same experiments on ONP100 from the other synthetic batch (batch A, see Fig. S11†), we did not quite explore such high excitation densities and did not observe the shortening of the excitons lifetime. Still, we retrieved $\gamma = 7000 \pm 1100$ m^3 ns^{-1} (without or

with PH), in reasonable agreement with the results obtained with batch B (Fig. 5).

Complementary transient absorption (TA) experiments (see ESI† for details) are carried out to retrieve the excited state absorption (ESA) spectrum and its overlap with the fluorescence spectrum in order to evaluate the Förster radius R_{ESA} associated with the energy transfer between two S_1 excited states. The TA data recorded with various excitation probabilities in the range 3% to 14%, are illustrated in Fig. 6. The negative contribution observed at wavelengths longer than 500 nm (Fig. 6(A)) is dominated by ground state bleach (GSB) and stimulated emission (SE), while excited state absorption (ESA) dominates the signal at shorter wavelengths. The negative band (GSB + SE) is observed to slightly deepen and red-shift by 1.35 ps. This is mostly attributed to the dynamic Stokes shift of the SE signal – also observed for rhodamine dyes in aqueous solution (not shown) – resulting from vibrational and solvent (here polymer) relaxation on this time scale in the excited state. In addition, inhomogeneous broadening of the ground state absorption band may contribute to a genuine red-shift of the GSB due to exciton transfer from higher-energy absorbing dyes to lower-energy absorbing dyes, already on the ps time scale in these ONPs. A significant GSB redshift was observed, although on a much slower time scale, in other dye-loaded PMMA films[85] and attributed to inhomogeneous spectral broadening. Following this early spectral relaxation, the TA signal decays already very significantly by 60 ps, indicating rapid EEA. With a pump pulse focused in the sample to a diameter of $\simeq 70$ μm, approximately twice as large as the diameter of the probe pulse, the decay kinetics compare very well with the data recorded with the SC in the presence of a pinhole, as illustrated in Fig. 6(B). This good agreement is also a consistency check for our evaluations of the excitation probabilities in both experimental setups. Provided that the large majority of
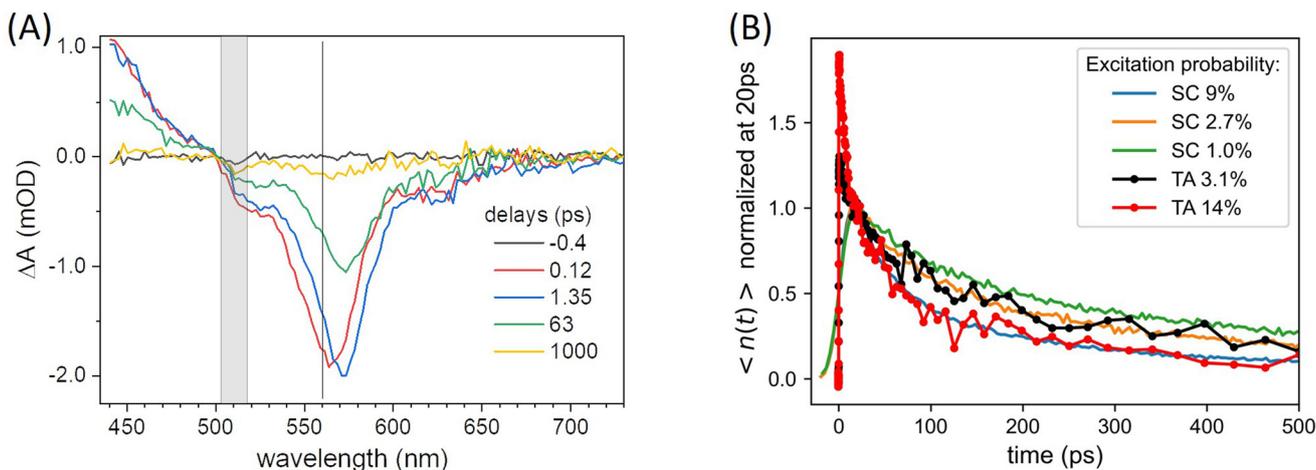

Fig. 6 Transient absorption (TA) spectroscopy on ONP30. (A) TA spectra (in mOD) at a selection of pump–probe delays (in ps), upon excitation at 515 nm with a 60 fs pulse and 3.1% excitation probability. The grey bar indicates the spectral region where pump light scattering degrades the signal quality. The vertical line at 560 nm indicates the ONP absorption maximum. (B) Comparison of the streak camera (SC) and TA kinetics recorded for various excitation probabilities. The TA kinetics are obtained by integrating the fluorescence signal spectrally from 550 nm to 730 nm.

excitons decays *via* EEA in the TA experiments, the formation with a 2% yield of a quencher state Q characterized by an extinction coefficient 5 times weaker than the SE and GSB signals, would contribute a positive signal of $\simeq 0.008$ mOD at maximum – in the same spectral range as the corresponding $\simeq -0.04$ mOD residual negative GSB. This remains undetectable in the present TA experiment characterized by a noise floor $\simeq 0.04$ mOD rms at 550 nm (evaluated at negative time delays, see *e.g.* the -0.4 ps signal in Fig. 6(A)), and further underlines the unparalleled sensitivity of the proposed confocal implementation of the photoluminescence experiment, as compared to a TA experiment.

The ESA spectrum can be extracted quantitatively from the TA signal observed on long times scales (*i.e.* after the early spectral relaxation) by subtracting the GSB and SE contributions. While the GSB is simply proportional to the opposite of the ground state absorption, the negative extinction coefficient for SE $\varepsilon_{SE}(\lambda)$ can be computed (in units of M^{-1} cm^{-1}) as (see ESI† for details):

$$\varepsilon_{SE}(\lambda) = -\frac{\int \frac{\varepsilon_{GS}(\lambda)}{\lambda} d\lambda}{\int A(\lambda)\lambda^3 d\lambda} A(\lambda)\lambda^4 \qquad (8)$$

where $\varepsilon_{GS}(\lambda)$ and $A(\lambda)$ are respectively the ground state extinction coefficient and the fluorescence emission spectrum displayed in Fig. 3(A). The retrieved ESA spectrum $\varepsilon_{ESA}(\lambda)$ is displayed in Fig. S14.† While its magnitude (ε_{ESA}^{max}) is evaluated with an error bar of $\pm 30\%$ (see ESI†), it strongly overlaps with the fluorescence emission $A(\lambda)$, resulting in a Förster radius $R_{EEA} = (1.10 \pm 0.05) \times R_0$, where R_0 is the Förster radius for homo-FRET defined by the overlap of $\varepsilon_{GS}(\lambda)$ with the same $A(\lambda)$ (see ESI† for details). The ESA spectrum retrieved here compares well with that of rhodamine B in ethanol,[86] and the reported $\varepsilon_{ESA}^{max} = 38\,000$ M^{-1} cm^{-1} falls within our error bar.

Discussion

In all kinetic traces reported in this work, the asymptotic decay corresponds to the 4.2 ns radiative lifetime of R18/F5-TPB in PMMA, except when the excitation power exceeds the threshold where EEA-induced byproducts start reducing the exciton lifetimes *via* collisional quenching (Fig. 5(C) and eqn (7)). We propose that also collisional quenching – itself boosted by large exciton diffusivity – is the mechanism for the onset of shorter-lived exciton sub-populations,[87] as a function of dye concentration (Fig. 3(B)). Increasing dye-loading most likely enhances the population of molecular aggregates possibly also acting as quenchers available for exciton collisional quenching. However, the fact that even at 100 wt% dye loading, about 20% of the exciton population has an unquenched lifetime would then reveal the presence of nanoparticles or sub-domains inside nanoparticles, where no quenching occurs. Conversely, the population of shorter-lived excitons would reveal various degrees of quenching probabilities as a function of the (small, hence fluctuating) number of effective quenchers

in ONPs. Together with the assumption of a homogeneous distribution of (R18/F5-TPB) inside ONPs, these considerations led us to define eqn (6) as a fitting function, where we postulate an average EEA rate γ, but a distribution of lifetimes, in fact revealing a distribution of quencher concentrations to collide with.

With $\gamma = 5600$ nm^3 ns^{-1} in ONP30 particles or domains where no quencher is present (*i.e.* $k^{-1} = 4.2$ ns), we find that the critical density above which EEA becomes significant is $n_A = 2k/\gamma = 8 \times 10^{-5}$ nm^{-3}. This corresponds to an average distance[88] between excitons of $0.554/n_A^{1/3} \sim 13$ nm $> 2R_{EEA}$, meaning that no "direct" EEA[57] may occur at such low densities. Instead, EEA is rather a diffusion-limited process, justifying *a posteriori* the fact that γ is time-independent. To further test this statement, we performed a simultaneous global fit (not shown) of the entire dataset illustrated in Fig. 6(B) including the relatively noisier TA data (with time delays from 1 ps on) together with the SC data (with time delays from 30 ps on) at all excitation powers realized in both experiments. The fit function was K_{PH} as given by eqn (6), and the fit quality was evaluated in terms of the reduced χ^2 weighted with the data noise distribution on each kinetic trace. The fit quality was neither improved when assuming a time-dependent EEA rate $\gamma(t) = a + b/\sqrt{t}$ as expected in case of direct energy transfer at very early time delays,[57,67] nor significantly degraded when keeping a time-independent γ fitting parameter.

We also note that with a dye number density $\rho = 0.1$ nm^{-3} for ONP30 – *i.e.* $\simeq 4000$ dyes per nanoparticle – the exciton density n_A corresponds to an excitation probability of 0.08%, *i.e.* no more than 3 to 4 excitons per nanoparticle. We conclude that exciton diffusion is efficient enough, that EEA occurs with significant probability with only few excitons inside a nanoparticle, provided no other quencher limits the excitons lifetime. Similarly, few energy acceptors or quenchers must be enough to cause collisional shortening of the exciton lifetime, as argued above, and in line with previous reports of a giant antenna effect enhancing the effective brightness of a single fluorescent acceptor in these ONPs,[38] or a collective fluorescence quenching in closely related ONPs (R18/F5-TPB in poly(D,L-lactide-*co*-glycolide) – PLGA – polymer).[35]

For biosensing applications, single ONP fluorescence spectroscopy is performed under cw illumination with light intensities in the range of 1 W cm^{-2} or lower.[32,38,89] Under such conditions (see ESI Section 8† for details), a 30 wt% loaded ONP absorbs photons with a rate in the MHz range, and we evaluate to ~ 10 Hz the frequency of EEA events. Hence, about 1 EEA-induced quencher state Q is produced every 5 seconds. The rates of EEA events and Q state production are 5 times larger in ONP100.

We now discuss how to infer a diffusion coefficient D from the measured, time-independent γ parameter. As mentioned in the introduction, we need to postulate a model for the diffusion-limited EEA process. In the following, we will postulate the validity of the Förster model which describes an incoherent energy transfer due to a resonant dipole–dipole interaction, because (i) the disorder and weak interactions between

the dyes are arguments in favor of the incoherent hoping assumption (*i.e.* we hypothesize, that there is no electronic excitation delocalisation among nearby chromophores), and (ii) the investigation of any other model is beyond the scope of this work. Unless numerical modeling is used, only two limiting cases can be discussed analytically: the low-diffusion limit, where direct energy transfer dominates, and the high-diffusion limit.[40,52,67,70,71] Following the above discussion, we shall consider the latter case.

The high-diffusion limit is commonly discussed based on the Smoluchovsky model for coagulation in colloids, where R_e is a contact radius introduced as a boundary condition in the diffusion equation.[67,88] As such, R_e defines a distance also called the radius of "dark sphere", at which EEA occurs with probability one at first encounter.[40,71] Very generally, R_e is postulated to be equal to the inter-dye distance and arbitrarily chosen to be $R_e = 1$ nm.[9,10,40,42,45,66,90]

An alternative approach to the dark sphere model describes the evolution of the exciton pair correlation function $g(\vec{r}, t)$, with:[52,69,70]

$$\gamma(t) = \int g(\vec{r}, t) k_{EEA}(r) d\vec{r}, \tag{9}$$

where $k_{EEA}(r)$ is the bimolecular annihilation rate as a function of inter-exciton distance, *i.e.* $k_{EEA}(r) = k(R_{EAA}/r)^6$ within the Förster model. In the high-diffusion limit, the pair correlation function relaxes rapidly and becomes time-independent. Introducing the hard sphere approximation with an effective interaction radius R_e ($g(r) = 0$ if $r < R_e$ and $g(r) = 1$ if $r \geq R_e$) results in:[70]

$$\gamma = \frac{4\pi}{3} k \frac{R_{EAA}^6}{R_e^3}. \tag{10}$$

In contrast to the dark sphere model, we argue that when two excitons approach at a distance as low as the inter-dye or "hopping" distance, they still have a non vanishing probability to hop on another ground state chromophore also available within the same distance – and to continue their diffusive motion – rather than to annihilate at first encounter. Therefore R_e may be defined as the inter-dye distance at which annihilation and further diffusion balance, by equating the typical times scales for exciton transport on distance R_e and energy transfer between excitons separated by R_e: $R_e^2/(2D) = 1/k_{EEA}(R_e)$.[52,71] As a result we get:

$$2D = \left(\frac{3\gamma}{4\pi}\right)^{4/3} k^{-1/3} R_{EEA}^{-2} \tag{11}$$

Here, we stress, that the relevant diffusion coefficient is $2D$ rather than D, because EEA occurs between two diffusing excitons, rather than between one mobile exciton and one fixed "trap" or quencher.[40,71,88] With $R_0 = 5.2$ nm (see ESI†) *i.e.* $R_{EEA} = 5.7$ nm, and $k^{-1} = 4.2$ ns we find for ONP30: $D = 370$ nm^2 ns^{-1}. With an average exciton lifetime of $\langle\tau\rangle = 2.35$ ns, this yields an exciton (3-dimensional) diffusion length $L = \sqrt{6D\langle\tau\rangle} \simeq 73$ nm. For ONP100, $\gamma \simeq 8000$ nm^2 ns^{-1} yields a

larger $D = 580$ nm^2 ns^{-1}, but the same $L = 75$ nm due to the slightly reduced $\langle\tau\rangle$ value.

In a disordered solution of dyes interacting *via* resonant dipole interaction with Förster radius R_0, incoherent exciton transport is predicted to become diffusive on a time scale shorter than the exciton lifetime k^{-1} provided the dimensionless concentration $C = \frac{4\pi}{3} R_0^3 \rho$ exceeds unity, with ρ the dye number density.[26] For the 30 wt% dye-loaded ONPs, we have $C \sim 60$ indicative of a fully diffusive transport. In such a case the diffusion coefficient is predicted to be:

$$D_{th} = \zeta \times kC^{4/3}R_0^2, \tag{12}$$

with ζ a dimensionless prefactor, the precise value of which (0.32, 0.43 or 0.56) has been the subject of various theoretical investigations.[26,70,91] With $\zeta = 0.5$ arbitrarily chosen, eqn (12) predicts $D_{th} = 700$ and 2000 nm^2 ns^{-1} for ONP30 and ONP100, respectively, *i.e.* a factor of 2 to 4 larger than the diffusion constant determined from the above EEA monitoring experiments. Extensive investigations of rigid solutions of perylene red in PMMA films[57,72,85,92–94] concluded that inhomogeneous spectral broadening explains a similar discrepancy between the measured diffusion coefficients and the values expected from eqn (12): after the first few exciton hopping events and simultaneous energy relaxation, the blue-most absorbing dyes would no longer contribute to electronic excitation transfer, thus reducing the concentration of dyes effectively available for excitation energy transport. Comparatively, the diffusion coefficient D measured in the present (R18/F5-TPB) loaded ONPs is one order of magnitude larger than in perylene red PMMA films[57] with same dye loadings,[57] and the saturation of the D value in ONP100 occurs at significantly larger dye concentration. We speculate, that the larger D value observed here may be due to a weaker effect of inhomogeneous broadening in the (R18/F5-TPB) dye/counterion system.

While we provide an accurate measurement of the EEA rate and sensitive detection of EEA by-products acting as quenchers, complementary theoretical investigation is required to refine the present evaluation of the exciton diffusion length, and to conclude whether the proposed incoherent hoping mechanism holds, or whether (transient) electronic excitation delocalization operates – like argued in natural LH complexes – to further enhance exciton transport properties also in disordered, rigid dye solutions at such large concentrations.

Conclusion

We report on EEA kinetics in dye-loaded ONPs dispersed in water solution, by monitoring photoluminescence decay kinetics as a function of excitation pulse intensity. We demonstrate that the inhomogeneous intensity profile of the excitation pulse has a very significant influence on the observed decay kinetics. While this effect is most generally overlooked, we show that it induces a systematic underestimate – possibly exceeding a factor of 3 depending on the actual pulse intensity profile – of the retrieved EEA rate γ, which also erroneously

appears to be intensity dependent. We propose two methods to solve this experimental issue. (i) We derive the functional form expected for the decay kinetics actually observed with a Gaussian excitation pulse profile and use it to fit the data. Alternatively, (ii) we implement a simple "confocal" experimental scheme (*i.e.* one pinhole in between two achromats). Only in the latter case can one use the expected eqn (2) to globally fit the observed decay kinetics and extract an unbiased γ value, independent of the pulse intensity. The confocal detection scheme also appears superior in detecting the EEA-induced formation of minor by-products inducing further exciton collisional quenching, a process which remains unnoticed when averaging the signal over the entire excitation volume.

With the present PMMA–MA ONPs loaded with rhodamine B dye derivatives (R18) and bulky F5-TPB counterions, we observe efficient EEA already at excitation probabilities as low as 0.1% – *i.e.* few excitons per ONP – indicating efficient exciton transport within the ONPs, in perfect line with the outstanding LH properties previously reported for these ONPs. The quantitative evaluation of the exciton diffusion constant and diffusion length is conditioned to the modeling of both exciton transport and exciton interactions in the ONPs. Assuming here incoherent exciton hopping and FRET between colliding excitons, we infer an exciton diffusion length in the range of 70 nm, *i.e.* almost twice the ONP diameter. This is a remarkably high value for a disordered, rigid solution of dyes, which results from (i) a diffusion coefficient exceeding that of other dye loaded PMMA films by one order of magnitude, and (ii) a relatively large exciton lifetime. Both properties are due to the ONP design strategy using bulky counterions to mitigate aggregation-caused fluorescence quenching even at large dye concentration (up to 0.3 M). The ONP100 explores the limits of the present synthetic design, since the exciton diffusion length does not exceed that of ONP30. In contrast with the quest for structurally ordered molecular systems possibly enabling exciton delocalization and quantum transport, this work adopts an alternative design strategy, which results in outstanding exciton transport in disordered assemblies of weakly interacting dyes in ONPs with remarkable, functional LH properties.

Conflicts of interest

The authors declare no conflict of interest.

Acknowledgements

References

1 R. Monshouwer, M. Abrahamsson, F. Van Mourik and R. Van Grondelle, Superradiance and exciton delocalization in bacterial photosynthetic light-harvesting systems, *J. Phys. Chem. B*, 1997, **101**(37), 7241–7248.

2 G. D. Scholes, G. R. Fleming, A. Olaya-Castro and R. van Grondelle, Lessons from nature about solar light harvesting, *Nat. Chem.*, 2011, **3**, 763–774.

3 T. Mirkovic, E. E. Ostroumov, J. M. Anna, R. van Grondelle, Govindjee and G. D. Scholes, Light Absorption and Energy Transfer in the Antenna Complexes of Photosynthetic Organisms, *Chem. Rev.*, 2017, **117**(2), 249–293.

4 J. Cao, R. J. Cogdell, D. F. Coker, H.-G. Duan, J. Hauer, U. Kleinekathöfer, T. L. C. Jansen, T. Mančal, R. J. D. Miller, J. P. Ogilvie, V. I. Prokhorenko, T. Renger, H.-S. Tan, R. Tempelaar, M. Thorwart, E. Thyrhaug, S. Westenhoff and D. Zigmantas, Quantum biology revisited, *Sci. Adv.*, 2020, **6**, eaaz4888.

5 A. Klinger, D. Lindorfer, F. Müh and T. Renger, Living on the edge: light-harvesting efficiency and photoprotection in the core of green sulfur bacteria, *Phys. Chem. Chem. Phys.*, 2023, **25**(28), 18698–18710.

6 O. V. Mikhnenko, P. W. M. Blom and T.-Q. Nguyen, Exciton diffusion in organic semiconductors, *Energy Environ. Sci.*, 2015, **8**(7), 1867–1888.

7 Y. Tamai, H. Ohkita, H. Benten and S. Ito, Exciton Diffusion in Conjugated Polymers: From Fundamental Understanding to Improvement in Photovoltaic Conversion Efficiency, *J. Phys. Chem. Lett.*, 2015, **6**, 3417–3428.

8 S. M. Menke, W. A. Luhman and R. J. Holmes, Tailored exciton diffusion in organic photovoltaic cells for enhanced power conversion efficiency, *Nat. Mater.*, 2013, **12**, 152–157.

9 S. Chandrabose, K. Chen, A. J. Barker, J. J. Sutton, S. K. K. Prasad, J. Zhu, J. Zhou, K. C. Gordon, Z. Xie, X. Zhan and J. M. Hodgkiss, High Exciton Diffusion Coefficients in Fused Ring Electron Acceptor Films, *J. Am. Chem. Soc.*, 2019, **141**, 6922–6929.

10 Y. Firdaus, V. M. Le Corre, S. Karuthedath, W. Liu, A. Markina, W. Huang, S. Chattopadhyay, M. M. Nahid, M. I. Nugraha, Y. Lin, A. Seitkhan, A. Basu, W. Zhang, I. McCulloch, H. Ade, J. Labram, F. Laquai, D. Andrienko, L. J. A. Koster and T. D. Anthopoulos, Long-range exciton diffusion in molecular non-fullerene acceptors, *Nat. Commun.*, 2020, **11**, 5220.

11 P. A. Hume, W. Jiao and J. M. Hodgkiss, Long-range exciton diffusion in a non-fullerene acceptor: approaching the incoherent limit, *J. Mater. Chem. C*, 2021, **9**(4), 1419–1428.

12 Y. Cai, Q. Li, G. Lu, H. S. Ryu, Y. Li, H. Jin, Z. Chen, Z. Tang, G. Lu, X. Hao, H. Y. Woo, C. Zhang and Y. Sun,

Vertically optimized phase separation with improved exciton diffusion enables efficient organic solar cells with thick active layers, *Nat. Commun.*, 2022, **13**, 2369.

13 H. Wang, S. Jin, X. Zhang and Y. Xie, Excitonic Effects in Polymeric Photocatalysts, *Angew. Chem., Int. Ed.*, 2020, **59**, 22828–22839.

14 Y. Zhu, Z. Zhang, W. Si, Q. Sun, G. Cai, Y. Li, Y. Jia, X. Lu, W. Xu, S. Zhang and Y. Lin, Organic Photovoltaic Catalyst with Extended Exciton Diffusion for High-Performance Solar Hydrogen Evolution, *J. Am. Chem. Soc.*, 2022, **144**, 12747–12755.

15 C. B. Winiger, S. Li, G. R. Kumar, S. M. Langenegger and R. Häner, Long-Distance Electronic Energy Transfer in Light-Harvesting Supramolecular Polymers, *Angew. Chem., Int. Ed.*, 2014, **53**, 13609–13613.

16 A. T. Haedler, K. Kreger, A. Issac, B. Wittmann, M. Kivala, N. Hammer, J. Köhler, H.-W. Schmidt and R. Hildner, Long-range energy transport in single supramolecular nanofibres at room temperature, *Nature*, 2015, **523**, 196–199.

17 X.-H. Jin, M. B. Price, J. R. Finnegan, C. E. Boott, J. M. Richter, A. Rao, S. M. Menke, R. H. Friend, G. R. Whittell and I. Manners, Long-range exciton transport in conjugated polymer nanofibers prepared by seeded growth, *Science*, 2018, **360**, 897–900.

18 C. Rehhagen, M. Stolte, S. Herbst, M. Hecht, S. Lochbrunner, F. Würthner and F. Fennel, Exciton Migration in Multistranded Perylene Bisimide J-Aggregates, *J. Phys. Chem. Lett.*, 2020, **11**(16), 6612–6617.

19 A. J. Sneyd, T. Fukui, D. Paleček, S. Prodhan, I. Wagner, Y. Zhang, J. Sung, S. M. Collins, T. J. A. Slater, Z. Andaji-Garmaroudi, L. R. MacFarlane, J. D. Garcia-Hernandez, L. Wang, G. R. Whittell, J. M. Hodgkiss, K. Chen, D. Beljonne, I. Manners, R. H. Friend and A. Rao, Efficient energy transport in an organic semiconductor mediated by transient exciton delocalization, *Sci. Adv.*, 2021, **7**, eabh4232.

20 S. Stäter, F. A. Wenzel, H. Welz, K. Kreger, J. Köhler, H.-W. Schmidt and R. Hildner, Directed Gradients in the Excited-State Energy Landscape of Poly(3-hexylthiophene) Nanofibers, *J. Am. Chem. Soc.*, 2023, **145**, 13780–13787.

21 K. Müller, K. S. Schellhammer, N. Gräßler, B. Debnath, F. Liu, Y. Krupskaya, K. Leo, M. Knupfer and F. Ortmann, Directed exciton transport highways in organic semiconductors, *Nat. Commun.*, 2023, **14**, 5599.

22 J. M. Moix, M. Khasin and J. Cao, Coherent quantum transport in disordered systems: I. The influence of dephasing on the transport properties and absorption spectra on one-dimensional systems, *New J. Phys.*, 2013, **15**, 085010.

23 T. Brixner, R. Hildner, J. Köhler, C. Lambert and F. Würthner, Exciton Transport in Molecular Aggregates – From Natural Antennas to Synthetic Chromophore Systems, *Adv. Energy Mater.*, 2017, **7**(16), 1700236.

24 W. Popp, D. Brey, R. Binder and I. Burghardt, Quantum Dynamics of Exciton Transport and Dissociation in Multichromophoric Systems, *Annu. Rev. Phys. Chem.*, 2021, **72**, 591–616.

25 F. Dubin, R. Melet, T. Barisien, R. Grousson, L. Legrand, M. Schott and V. Voliotis, Macroscopic coherence of a single exciton state in an organic quantum wire, *Nat. Phys.*, 2006, **2**, 32–35.

26 C. R. Gochanour, H. C. Andersen and M. D. Fayer, Electronic excited state transport in solution, *J. Chem. Phys.*, 1979, **70**(9), 4254–4271.

27 B. Wittmann, F. A. Wenzel, S. Wiesneth, A. T. Haedler, M. Drechsler, K. Kreger, J. Köhler, E. W. Meijer, H.-W. Schmidt and R. Hildner, Enhancing Long-Range Energy Transport in Supramolecular Architectures by Tailoring Coherence Properties, *J. Am. Chem. Soc.*, 2020, **142**, 8323–8330.

28 V. I. Novoderezhkin and R. van Grondelle, Physical origins and models of energy transfer in photosynthetic light-harvesting, *Phys. Chem. Chem. Phys.*, 2010, **12**(27), 7352.

29 S. Giannini, W.-T. Peng, L. Cupellini, D. Padula, A. Carof and J. Blumberger, Exciton transport in molecular organic semiconductors boosted by transient quantum delocalization, *Nat. Commun.*, 2022, **13**, 2755.

30 D. Balzer and I. Kassal, Mechanism of Delocalization-Enhanced Exciton Transport in Disordered Organic Semiconductors, *J. Phys. Chem. Lett.*, 2023, **14**, 2155–2162.

31 A. Reisch and A. S. Klymchenko, Fluorescent Polymer Nanoparticles Based on Dyes: Seeking Brighter Tools for Bioimaging, *Small*, 2016, **12**, 1968–1992.

32 D. S. Biswas, P. Gaki, E. C. Da Silva, A. Combes, A. Reisch, P. Didier and A. S. Klymchenko, Long-range Energy Transfer Between Dye-loaded Nanoparticles: Observation and Amplified Detection of Nucleic Acids, *Adv. Mater.*, 2023, 2301402.

33 I. Shulov, S. Oncul, A. Reisch, Y. Arntz, M. Collot, Y. Mely and A. S. Klymchenko, Fluorinated counterion-enhanced emission of rhodamine aggregates: ultrabright nanoparticles for bioimaging and light-harvesting, *Nanoscale*, 2015, **7**(43), 18198–18210.

34 A. H. Ashoka, I. O. Aparin, A. Reisch and A. S. Klymchenko, Brightness of fluorescent organic nanomaterials, *Chem. Soc. Rev.*, 2023, **52**(14), 4525–4548.

35 A. Reisch, P. Didier, L. Richert, S. Oncul, Y. Arntz, Y. Mély and A. S. Klymchenko, Collective fluorescence switching of counterion-assembled dyes in polymer nanoparticles, *Nat. Commun.*, 2014, **5**, 4089.

36 H. Lin, R. Camacho, Y. Tian, T. E. Kaiser, F. Würthner and I. G. Scheblykin, Collective Fluorescence Blinking in Linear J-Aggregates Assisted by Long-Distance Exciton Migration, *Nano Lett.*, 2010, **10**(2), 620–626.

37 A. Reisch, K. Trofymchuk, A. Runser, G. Fleith, M. Rawiso and A. S. Klymchenko, Tailoring Fluorescence Brightness and Switching of Nanoparticles through Dye Organization in the Polymer Matrix, *ACS Appl. Mater. Interfaces*, 2017, **9**(49), 43030–43042.

38 K. Trofymchuk, A. Reisch, P. Didier, F. Fras, P. Gilliot, Y. Mely and A. S. Klymchenko, Giant light-harvesting

nanoantenna for single-molecule detection in ambient light, *Nat. Photonics*, 2017, **11**, 657–663.

39 N. Melnychuk, S. Egloff, A. Runser, A. Reisch and A. S. Klymchenko, Light-Harvesting Nanoparticle Probes for FRET-Based Detection of Oligonucleotides with Single-Molecule Sensitivity, *Angew. Chem., Int. Ed.*, 2020, **59**(17), 6811–6818.

40 R. C. Powell and Z. G. Soos, Singlet exciton energy transfer in organic solids, *J. Lumin.*, 1975, **11**(1–2), 1–45.

41 J. D. A. Lin, O. V. Mikhnenko, J. Chen, Z. Masri, A. Ruseckas, A. Mikhailovsky, R. P. Raab, J. Liu, P. W. M. Blom, M. A. Loi, C. J. García-Cervera, I. D. W. Samuel and T.-Q. Nguyen, Systematic study of exciton diffusion length in organic semiconductors by six experimental methods, *Mater. Horiz.*, 2014, **1**(2), 280–285.

42 M. A. Stevens, C. Silva, D. M. Russell and R. H. Friend, Exciton dissociation mechanisms in the polymeric semi-conductors poly(9,9-dioctylfluorene) and poly(9,9-dioctyl-fluorene-co-benzothiadiazole), *Phys. Rev. B: Condens. Matter Mater. Phys.*, 2001, **63**(16), 165213.

43 A. Lewis, A. Ruseckas, O. Gaudin, G. Webster, P. Burn and I. Samuel, Singlet exciton diffusion in MEH-PPV films studied by exciton–exciton annihilation, *Org. Electron.*, 2006, **7**, 452–456.

44 P. E. Shaw, A. Ruseckas and I. D. W. Samuel, Exciton Diffusion Measurements in Poly(3-hexylthiophene), *Adv. Mater.*, 2008, **20**(18), 3516–3520.

45 S. Cook, H. Liyuan, A. Furube and R. Katoh, Singlet Annihilation in Films of Regioregular Poly(3-hexylthio-phene): Estimates for Singlet Diffusion Lengths and the Correlation between Singlet Annihilation Rates and Spectral Relaxation, *J. Phys. Chem. C*, 2010, **114**, 10962–10968.

46 S. Kumar, I. S. Dunn, S. Deng, T. Zhu, Q. Zhao, O. F. Williams, R. Tempelaar and L. Huang, Exciton annihilation in molecular aggregates suppressed through quantum interference, *Nat. Chem.*, 2023, **15**, 1118–1126.

47 C. G. Hübner, G. Zumofen, A. Renn, A. Herrmann, K. Müllen and T. Basché, Photon Antibunching and Collective Effects in the Fluorescence of Single Bichromophoric Molecules, *Phys. Rev. Lett.*, 2003, **91**(9), 093903.

48 J. Hofkens, M. Cotlet, T. Vosch, P. Tinnefeld, K. D. Weston, C. Ego, A. Grimsdale, K. Mullen, D. Beljonne, J. L. Bredas, S. Jordens, G. Schweitzer, M. Sauer and F. De Schryver, Revealing competitive Forster-type resonance energy-trans-fer pathways in single bichromophoric molecules, *Proc. Natl. Acad. Sci. U. S. A.*, 2003, **100**(23), 13146–13151.

49 D. Nettels, D. Haenni, S. Maillot, M. Gueye, A. Barth, V. Hirschfeld, C. G. Hubner, J. Léonard and B. Schuler, Excited-state annihilation reduces power dependence of single-molecule FRET experiments, *Phys. Chem. Chem. Phys.*, 2015, **17**(48), 32304–32315.

50 G. J. Hedley, T. Schröder, F. Steiner, T. Eder, F. J. Hofmann, S. Bange, D. Laux, S. Höger, P. Tinnefeld, J. M. Lupton and J. Vogelsang, Picosecond time-resolved photon antibunch-

ing measures nanoscale exciton motion and the true number of chromophores, *Nat. Commun.*, 2021, **12**, 1327.

51 L. Valkunas, G. Trinkunas, V. Liuolia and R. Van Grondelle, Nonlinear annihilation of excitations in photosynthetic systems, *Biophys. J.*, 1995, **69**, 1117–1129.

52 V. Gulbinas, M. Chachisvilis, L. Valkunas and V. Sundström, Excited State Dynamics of Phthalocyanine Films, *J. Phys. Chem.*, 1996, **100**(6), 2213–2219.

53 G. Trinkunas, J. L. Herek, T. Polívka, V. Sundström and T. Pullerits, Exciton Delocalization Probed by Excitation Annihilation in the Light-Harvesting Antenna LH2, *Phys. Rev. Lett.*, 2001, **86**(18), 4167–4170.

54 E. Engel, K. Leo and M. Hoffmann, Ultrafast relaxation and exciton–exciton annihilation in PTCDA thin films at high excitation densities, *Chem. Phys.*, 2006, **325**(1), 170–177.

55 V. Gulbinas, I. Minevičiūtė, D. Hertel, R. Wellander, A. Yartsev and V. Sundström, Exciton diffusion and relax-ation in methyl-substituted polyparaphenylene polymer films, *J. Chem. Phys.*, 2007, **127**(14), 144907.

56 S. M. King, D. Dai, C. Rothe and A. P. Monkman, Exciton annihilation in a polyfluorene: Low threshold for singlet-singlet annihilation and the absence of singlet-triplet annihilation, *Phys. Rev. B: Condens. Matter Mater. Phys.*, 2007, **76**(8), 085204.

57 F. Fennel and S. Lochbrunner, Exciton-exciton annihilation in a disordered molecular system by direct and multistep Förster transfer, *Phys. Rev. B: Condens. Matter Mater. Phys.*, 2015, **92**, 140301.

58 S. E. Bradforth, R. Jimenez, F. van Mourik, R. van Grondelle and G. R. Fleming, Excitation Transfer in the Core Light-Harvesting Complex (LH-1) of Rhodobacter sphaeroides: An Ultrafast Fluorescence Depolarization and Annihilation Study, *J. Phys. Chem.*, 1995, **99**(43), 16179–16191.

59 H. Wang, H.-Y. Wang, B.-R. Gao, L. Wang, Z.-Y. Yang, X.-B. Du, Q.-D. Chen, J.-F. Song and H.-B. Sun, Exciton diffusion and charge transfer dynamics in nano phase-sep-arated P3HT/PCBM blend films, *Nanoscale*, 2011, **3**(5), 2280.

60 J. Dostál, F. Fennel, F. Koch, S. Herbst, F. Würthner and T. Brixner, Direct observation of exciton–exciton inter-actions, *Nat. Commun.*, 2018, **9**(1), 2466.

61 P. Malý, J. Lüttig, A. Turkin, J. Dostál, C. Lambert and T. Brixner, From wavelike to sub-diffusive motion: exciton dynamics and interaction in squaraine copolymers of varying length, *Chem. Sci.*, 2020, **11**(2), 456–466.

62 P. Malý, J. Lüttig, P. A. Rose, A. Turkin, C. Lambert, J. J. Krich and T. Brixner, Separating single- from multi-par-ticle dynamics in nonlinear spectroscopy, *Nature*, 2023, **616**(7956), 280–287.

63 A. Dogariu, D. Vacar and A. J. Heeger, Picosecond time-resolved spectroscopy of the excited state in a soluble derivative of poly(phenylene vinylene): Origin of the bimo-lecular decay, *Phys. Rev. B: Condens. Matter Mater. Phys.*, 1998, **58**(16), 10218–10224.

64 M. Kirm, V. Nagirnyi, E. Feldbach, M. De Grazia, B. Carré, H. Merdji, S. Guizard, G. Geoffroy, J. Gaudin, N. Fedorov, P. Martin, A. Vasil'ev and A. Belsky, Exciton-exciton interactions in CdWO$_4$ irradiated by intense femtosecond vacuum ultraviolet pulses, *Phys. Rev. B: Condens. Matter Mater. Phys.*, 2009, **79**(23), 233103.

65 A. Gharbi and J. Léonard, *EEA_Photolum*, 2024, **https://hal.archives-ouvertes.fr/hal-04561022**.

66 Y. Zaushitsyn, K. G. Jespersen, L. Valkunas, V. Sundström and A. Yartsev, Ultrafast dynamics of singlet-singlet and singlet-triplet exciton annihilation in poly(3-2′-methoxy-5′-octylphenyl)thiophene films, *Phys. Rev. B: Condens. Matter Mater. Phys.*, 2007, **75**, 195201.

67 U. Gösele, M. Hauser, U. Klein and R. Frey, Diffusion and long-range energy transfer, *Chem. Phys. Lett.*, 1975, **34**, 519–522.

68 R. Tempelaar, T. L. C. Jansen and J. Knoester, Exciton–Exciton Annihilation Is Coherently Suppressed in H-Aggregates, but Not in J-Aggregates, *J. Phys. Chem. Lett.*, 2017, **8**, 6113–6117.

69 A. Suna, Kinematics of Exciton-Exciton Annihilation in Molecular Crystals, *Phys. Rev. B: Solid State*, 1970, **1**(4), 1716–1739.

70 S. Jang, K. J. Shin and S. Lee, Effects of excitation migration and translational diffusion in the luminescence quenching dynamics, *J. Chem. Phys.*, 1995, **102**, 815–827.

71 V. M. Agranovich and M. D. Galanin, *Electronic Excitation Energy Transfer in Condensed Matter*, North-Holland Publishing Company, 1982.

72 K. A. Colby, J. J. Burdett, R. F. Frisbee, L. Zhu, R. J. Dillon and C. J. Bardeen, Electronic Energy Migration on Different Time Scales: Concentration Dependence of the Time-Resolved Anisotropy and Fluorescence Quenching of Lumogen Red in Poly(methyl methacrylate), *J. Phys. Chem. A*, 2010, **114**(10), 3471–3482.

73 R. P. Haugland, *Handbook of fluorescent probes and research chemicals*, Molecular Probes, Eugene, 1996, vol. 8.

74 V. Klimov, D. McBranch, N. Barashkov and J. Ferraris, Biexcitons in π-conjugated oligomers: Intensity-dependent femtosecond transient-absorption study, *Phys. Rev. B: Condens. Matter Mater. Phys.*, 1998, **58**(12), 7654.

75 B. Kraabel, V. I. Klimov, R. Kohlman, S. Xu, H.-L. Wang and D. W. McBranch, Unified picture of the photoexcitations in phenylene-based conjugated polymers: Universal spectral and dynamical features in subpicosecond transient absorption, *Phys. Rev. B: Condens. Matter Mater. Phys.*, 2000, **61**, 8501–8515.

76 G. Denton, N. Tessler, M. Stevens and R. Friend, Optical response of conjugated polymers excited at high intensity, *Synth. Met.*, 1999, **102**, 1008–1009.

77 S. V. Frolov, Z. Bao, M. Wohlgenannt and Z. V. Vardeny, Ultrafast Spectroscopy of Even-Parity States in π-Conjugated Polymers, *Phys. Rev. Lett.*, 2000, **85**(10), 2196–2199.

78 C. Silva, A. S. Dhoot, D. M. Russell, M. A. Stevens, A. C. Arias, J. D. MacKenzie, N. C. Greenham, R. H. Friend, S. Setayesh and K. Müllen, Efficient exciton dissociation via two-step photoexcitation in polymeric semiconductors, *Phys. Rev. B: Condens. Matter Mater. Phys.*, 2001, **64**, 125211.

79 V. Gulbinas, Y. Zaushitsyn, H. Bässler, A. Yartsev and V. Sundström, Dynamics of charge pair generation in ladder-type poly(para-phenylene) at different excitation photon energies, *Phys. Rev. B: Condens. Matter Mater. Phys.*, 2004, **70**, 035215.

80 B. Kraabel, D. Hulin, C. Aslangul, C. Lapersonne-Meyer and M. Schott, Triplet exciton generation, transport and relaxation in isolated polydiacetylene chains: Subpicosecond pump-probe experiments, *Chem. Phys.*, 1998, **227**, 83–98.

81 M. Wohlgenannt, W. Graupner, G. Leising and Z. V. Vardeny, Photogeneration and recombination processes of neutral and charged excitations in films of a ladder-type poly(para-phenylene), *Phys. Rev. B: Condens. Matter Mater. Phys.*, 1999, **60**, 5321–5330.

82 C. Eggeling, A. Volkmer and C. A. M. Seidel, Molecular Photobleaching Kinetics of Rhodamine 6G by One- and Two-Photon Induced Confocal Fluorescence Microscopy, *ChemPhysChem*, 2005, **6**, 791–804.

83 R. Zondervan, F. Kulzer, S. B. Orlinskii and M. Orrit, Photoblinking of Rhodamine 6G in Poly(vinyl alcohol): Radical Dark State Formed through the Triplet, *J. Phys. Chem. A*, 2003, **107**(35), 6770–6776.

84 A. Dunne and M. F. Quinn, Triplet–triplet absorption spectra and the spectra of the photoreduced states of Rhodamine B and Rhodamine 110, *J. Chem. Soc., Faraday Trans. 1*, 1977, **73**, 1104.

85 F. Fennel and S. Lochbrunner, Förster-mediated spectral diffusion in disordered organic materials, *Phys. Rev. B: Condens. Matter Mater. Phys.*, 2012, **85**(9), 094203.

86 P. C. Beaumont, D. G. Johnson and B. J. Parsons, Excited state and free radical properties of rhodamine dyes in aqueous solution: A laser flash photolysis and pulse radiolysis study, *J. Photochem. Photobiol., A*, 1997, **107**(1–3), 175–183.

87 G. Fanciullo, I. Conti, P. Didier, A. Klymchenko, J. Léonard, M. Garavelli and I. Rivalta, Modelling quenching mechanisms of disordered molecular systems in the presence of molecular aggregates, *Phys. Chem. Chem. Phys.*, 2022, **24**, 1787–1794.

88 S. Chandrasekhar, Stochastic problems in physics and astronomy, *Rev. Mod. Phys.*, 1943, **15**(1), 1.

89 A. Reisch, A. Runser, Y. Arntz, Y. Mély and A. S. Klymchenko, Charge-Controlled Nanoprecipitation as a Modular Approach to Ultrasmall Polymer Nanocarriers: Making Bright and Stable Nanoparticles, *ACS Nano*, 2015, **9**(5), 5104–5116.

90 C. Rehhagen, S. Rafiq, K. N. Schwarz, G. D. Scholes and S. Lochbrunner, The effect of intermolecular electronic coupling on the exciton dynamics in perylene red nanoparticles, *Phys. Chem. Chem. Phys.*, 2022, **24**(15), 8695–8704.

91 S. W. Haan and R. Zwanzig, Förster migration of electronic excitation between randomly distributed molecules, *J. Chem. Phys.*, 1978, **68**(4), 1879–1883.

92 M. Schlosser and S. Lochbrunner, Exciton Migration by Ultrafast Förster Transfer in Highly Doped Matrixes, *J. Phys. Chem. B*, 2006, **110**(12), 6001–6009.

93 F. Fennel and S. Lochbrunner, Long distance energy transfer in a polymer matrix doped with a perylene dye, *Phys. Chem. Chem. Phys.*, 2011, **13**(8), 3527.

94 K. A. Colby and C. J. Bardeen, Electronic Energy Migration in Solid versus Liquid Host Matrices for Concentrated Perylenediimide Dye Solutions, *J. Phys. Chem. A*, 2011, **115**(26), 7574–7581.